Internal reflections and nonlinear effects interplay in non-ideal Josephson Travelling Wave Parametric Amplifiers

Internal reflections and nonlinear effects interplay in non-ideal JTWPA

Luca Fasolo (DET - Politecnico di Torino, Torino, Italy)

Luca Oberto (INRiM, Torino, Italy)

Luca Callegaro (INRiM, Torino, Italy)

Emanuele Enrico (INRiM, Torino, Italy)

Abstract:

The paper investigates the interplay of nonlinear effects with the non-ideal transmission properties of a Josephson Travelling Wave Parametric Amplifier (JTWPA). Experimental characterization using a microwave and DC cryogenic setup reveals periodic transmission modulation linked to the tuning of the Josephson inductances embedded in the line. The effects of impedance matching and resonant parametric down-conversion (PDC) are observed on a broadband scale, and the impact of design parameters and fabrication issues on device performance is analyzed. These findings contribute to the optimizing techniques for JTWPA devices, advancing quantum-limited amplifiers.

Introduction

Josephson Travelling Wave Parametric Amplifiers (JTWPA) have emerged as promising devices for low-noise amplification [1]–[4] and non-classical radiation manipulation [5], [6] in superconducting circuits. JTWPAs exploit the nonlinearity of Josephson junctions to achieve ultralow-noise wideband microwave amplification. In practical implementations, JTWPA device non-idealities can limit their overall performance [7], [8]. The aim of this paper is to explore nonlinear effects in non-ideal rf-SQUIDs and Resonant Phase-Matching (RPM) -based JTWPA devices [9]–[11] and to study the influence of key design parameters in transmission and mixing process ripples by investigating strategies to experimentally extrapolate as-built device parameters and by quantifying their adverse effects.

Readout circuit

The room temperature experimental setup is shown in Fig. 1. A low-budget microwave generator with two output channels generates tones in the 10 MHz to 24 GHz range, with output power to + 20 dBm. Isolators in the output lines prevent power reflections; bandpass and lowpass filters attenuate unwanted harmonics and sub-harmonics. The filtered pump and signal tones were combined using an ultrawideband power combiner. A directional coupler inserted on the signal path allows signal monitoring. The combined signals enter the input signal lines of a dilution refrigerator (DR) with a base temperature of 60 mK and reach the JTWPA after a proper attenuator chain (60 dB in total) that washes out room temperature noise components. Two cryogenic switches serve for calibration purposes [12]. The JTWPA output signal passes a 60 dB isolator stage located at 60 mK and is then amplified by a low-noise HEMT located at the 3 K stage of the DR. Eventually, it was acquired using a spectrum analyzer. The JTWPA under investigation is composed by an array of rf-SQUIDS cells and lumped element phase-matchers [8]. Its working point is tuned by a DC current I_{dc}, generated by a room-temperature source and injected in the JTWPA by properly filtered DC lines entering two cryogenic bias tees. For more details on the JTWPA parameters refer to [8].

Cryogenic Characterisation

A. Single Tone Transmission Spectroscopy

An initial single-tone measurement was performed to evaluate the JTWPA attenuation within the 4 GHz to 12 GHz range with negligible mixing effect by exploiting small probe signal respect to the Josephson nonlineariry. Figure 2 illustrates the $|S_{21}|$ spectrum of the tested JTWPA prototype as a function of the bias current I_{dc}. The relationship between the measured attenuation and the bias current exhibits a complex behavior, particularly for specific bias current values. However, a periodic trend in the spectrum relative to I_{dc} was observed, with a period of approximately $\tilde{I}_{dc} = 44.5$ µA across all frequencies.
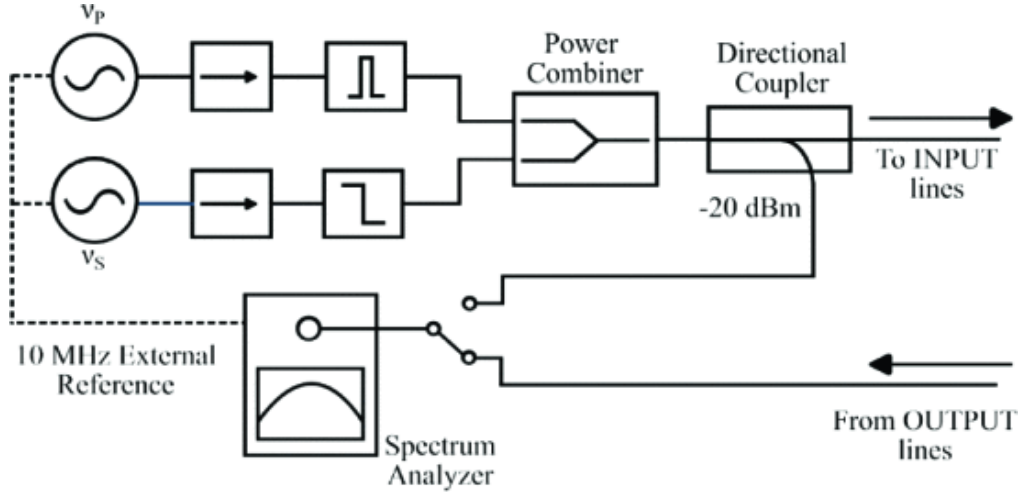
Fig. 1.
Schematic representation of the room temperature microwave circuit exploited for the characterization of the JTWPA prototype. See description in Sec. II.
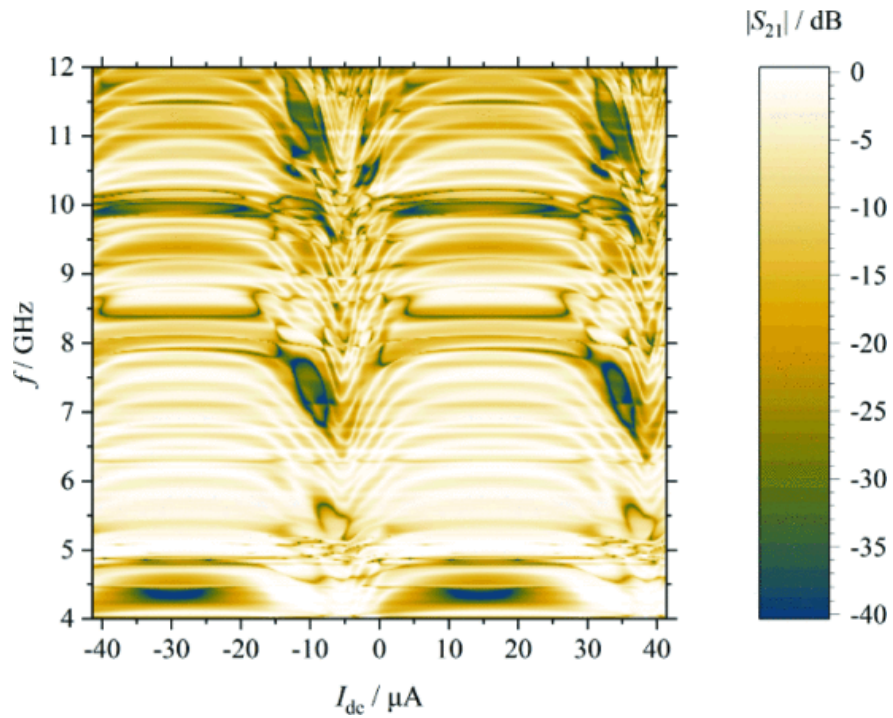
Fig. 2.
Measurement of $|S_{21}|$ (corrected for signal path losses) versus the bias current I_{dc} of the JTWPA under test.

Additionally, an offset was present in relation to the null current value, approximately at $I_{dc}^{off} = 14.7\,\mu A$. This offset is likely caused by a residual static magnetic flux bias inducing a flux offset across the rf-SQUIDs incompletely shielded by the μ-metal shield surrounding the cryogenic apparatus. The observed periodic modulation pattern in S_{21} versus I_{dc} can be attributed to the periodic variation of the Josephson inductances ($L_J(\Phi_{dc})$) integrated into the transmission line. The relationship between the bias current and the flux bias (Φ_{dc}) follows the description provided in the transcendental equation $I_{dc} = \frac{\Phi_{dc}}{L_g} + I_c \sin\left(2\pi \frac{\Phi_{dc}}{\Phi_0}\right)$.

In the case of a current-biased rf-SQUID, the periodic modulation arises due to the quantization of magnetic flux in a superconducting loop, resulting in a current period of $\tilde{I}_{dc} = \Phi_0/L_g$. Here, Φ_0 represents the magnetic flux quantum, and L_g corresponds to the geometric inductance of the superconducting loop [13]. Analyzing the measured $\tilde{I}_{dc}$, we determined that the effective geometric inductances of the implemented rf-SQUIDs within the JTWPA prototype are $L_{g,meas} \approx 46.5$ pH.

B. Toy-model describing internal reflections effects

The spectrum reported in Figure 2 exhibits minor attenuation due to relatively good impedance matching, except in localized regions. The average attenuation values increase with frequency, consistent with the expected behavior of a transmission line. Notably, the attenuation displays noticeable ripples, some of which are dependent on the bias current while others are not. The current-dependent modulations observed in Figure 2 directly result from the varying matching conditions between different segments of the parametric amplifier, as the characteristic impedance of an array of rf-SQUIDs varies with the bias current. To illustrate this assumption, a simplified model of the system, as depicted in Figure 3.a, can be considered.
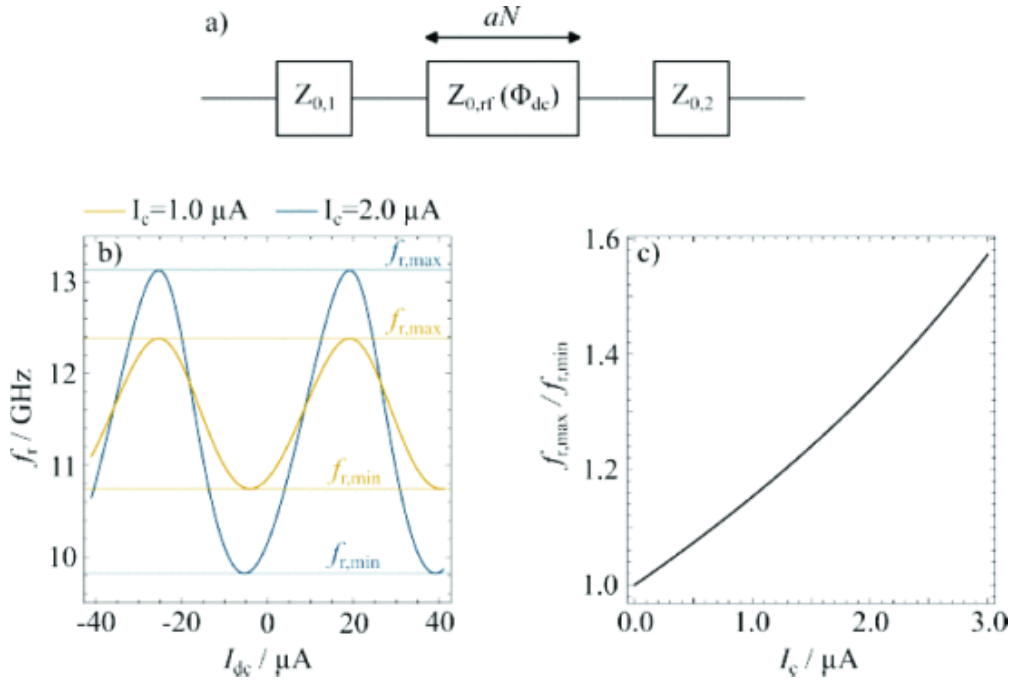
Fig. 3.
a) Pictorial representation of the simplified model used to interpret the ripples in $|S_{21}|$ generated by bias-dependent internal resonances. b) Bias-dependent resonant frequencies of a repetition of $N = 80$ rf-SQUIDs having a spatial periodicity of $a = 80\ \mu m$ for two different values of their Josephson junctions' critical current. For this numerical simulation $L_g = L_{g,exp} = 46.5$ pH and $C_g = 25$ fF. c) Relationship between the ratio $f_{r,max}/f_{r,min}$ and the critical current of the Josephson junctions for $L_g = L_{g,exp}$.

This toy model comprises a chain of current-biased identical rf-SQUIDs with a variable characteristic impedance denoted as $Z_{0,\text{rf}}(\Phi_{\text{dc}})$. The chain is positioned between two sections of a transmission line with different characteristic impedances, $Z_{0,1}$ and $Z_{0,2}$, which can either remain constant or be modulated by external bias. When the bias is such that $Z_{0,\text{rf}}(\Phi_{\text{dc}}) \neq Z_{0,1}$ and $Z_{0,\text{rf}}(\Phi_{\text{dc}}) \neq Z_{0,2}$ a resonance arises within the rf-SQUID chain due to multiple reflections induced by the mismatch conditions at the chain boundaries. The resonance frequency is dependent on the length of the chain and the value of its characteristic impedance, $f_r = f_r(\Phi_{\text{dc}})$. Considering a chain of N rf-SQUIDs spaced at a distance a from each other, the n-th resonant harmonic is given by:

$$f_{\text{r}}\left(\Phi_{\text{dc}}\right) = n\frac{v_{\text{ph}}\left(\Phi_{\text{dc}}\right)}{2aN},$$

Here, $v_{\text{ph}}\left(\Phi_{\text{dc}}\right) = a/\sqrt{L(\Phi_{\text{dc}})C_{\text{g}}}$ represents the bias-dependent phase velocity, $L(\Phi_{\text{dc}})=(L_{\text{g}}^{-1}+L_{\text{J}}^{-1}(\Phi_{\text{dc}}))^{-1}$ represents the bias-dependent total inductance of an rf-SQUID, and L_{g} is the geometric inductance of the superconducting loop. The phase velocity reaches its maximum when the current bias induces a static flux bias $\Phi_{\text{dc}} = 0$ and its minimum when $\Phi_{\text{dc}} = \pm\Phi_0/2$. Continuous variations in the bias current induce corresponding changes in the phase velocity and, consequently, in the resonant frequency of the chain. Figure 3.b illustrates this variation for the specific experimental parameters mentioned in the caption. It is worth emphasizing that the ratio between the maximum and minimum values of the resonance frequency, achieved in a chain with a fixed length due to its impedance variation, is determined exclusively by the geometric inductance and the critical current of the junctions, as indicated by the formula:

$$\frac{f_{\text{r,max}}}{f_{\text{r,min}}} = \frac{v_{\text{ph}}(0)}{v_{\text{ph}}(\pm\Phi_0/2)} = \sqrt{\frac{\varphi_0/I_{\text{c}} + L_{\text{g}}}{\varphi_0/I_{\text{c}} - L_{\text{g}}}}.$$

Figure 3.c presents this ratio for different values of I_c, considering $L_g = L_{\text{g,exp}}$. Through a qualitative analysis of the ratio between the maximum and minimum frequencies in each continuous ripple of $|S_{2,1}|$, a rough estimation of the critical currents of the Josephson junctions embedded in the fabricated JTWPA can be obtained, yielding approximately $I_{\text{c,exp}} = 1.5$ µA. Furthermore, this estimation leads to an estimation of the effective screening parameter $\beta_{\text{L}} = I_c L_g/\varphi_0 \approx 0.28$ governing the nonlinear phenomena in the rf-SQUID-based JTWPA.
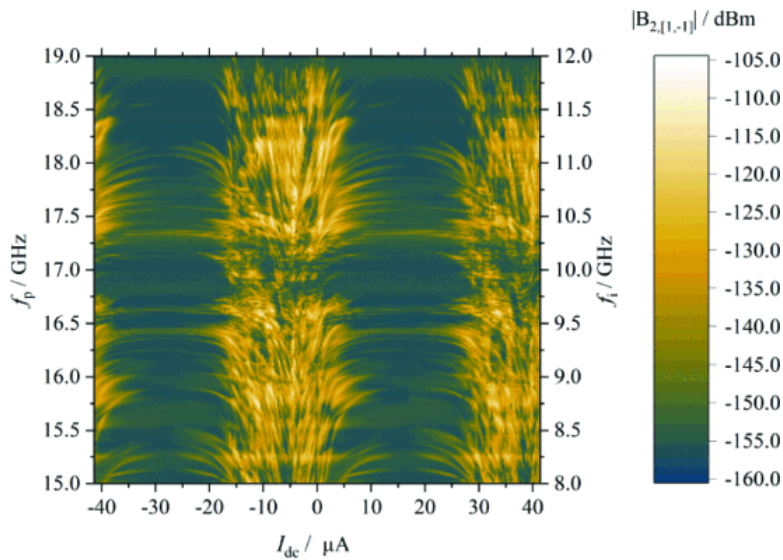
Fig. 4.
3WM idler power $|B_{2,[1,-1]}|$ at the parametric amplifier output port as a function of both the bias current I_{dc} and the pump frequency f_p. The right-axis reports the corresponding 3WM idler frequency $f_i = f_p - f_s$ for the fixed value $f_s = 7$ GHz.

C. Double tone spectroscopy reveals internal reflections enhanced mixing

By exploiting the Josephson nonlinearity, the mixing response of the JTWPA was evaluated by simultaneously introducing a fixed-frequency signal tone at 7 GHz and a variable-frequency pump tone in the 15 − 19 GHz range. Proper calibration of the signal power at the input port of the amplifier is estimated by exploiting a variable-temperature load calibration procedure. Using software automatization, the spectrum analyzer was controlled to measure, for each pump frequency value, the power generated at the corresponding 3WM idler frequency $f_i = f_p − f_s$. Figure 4 displays the idler frequency power at the output port of the amplifier as a function of the bias current. This quantity is labeled in the figure as $B_{2,[1,-1]}$ according to the Poly Harmonic Dispersion model [1] for the scattering of waves generated in nonlinear networks by the combinations of incommensurate frequencies. The $B_{2,[1,-1]}$ spectrum clearly highlights the occurrence of an idler photon generation through a 3WM PDC process. The modulated patterns in the spectrum, depending on the current bias values, closely resemble those observed in Figure 2, with a maximum generation of idler photons in correspondence with the conditions of higher attenuation. Considering the interpretation previously given for the $|S_{21}|$ spectrum in terms of multiple internal reflections, this close correspondence suggests that the main mechanism underlying this process is a resonant amplification of the generated idler photons.

Conclusions

In conclusion, the characterization of the first rf-SQUID-based JTWPA developed at INRiM has provided valuable insights for improving future realizations. The limited predictability of the fabricated Josephson junctions parameters driving the device nonlinearity appears to be the main bottleneck in producing parametric amplifiers with effective amplifying properties. Future investigations on further optimized devices will concentrate on the proper evaluation of the 1-dB compression point optimal pump power. The measurement of the modulations in the signal transmission induced by the bias current has confirmed some of the design parameters obtained through finite element simulations and the calibration of the fabrication protocol (eg. L_g, I_c, and β_L). Future activities will concentrate on the reproducibility of the fabrication of the Josephson junctions and will pave the way for reaching quantum-limited rf-SQUIDs-based JTWPAs.

1.
D.E. Root, J. Verspecht, D. Sharrit, J. Wood and A. Cognata, "Broadband polyharmonic distortion (phd) behavioral models from fast automated simulations and large-signal vectorial network measurements", *IEEE Transactions on Microwave Theory and Techniques*, vol. 53, no. 11, pp. 3656-3664, 2005.
2.
S. Pagano et al., "Development of Quantum Limited Superconducting Amplifiers for Advanced Detection", *IEEE Transactions on Applied Superconductivity*, vol. 32, no. 4, pp. 1-5, June 2022.
3.
L. Fasolo, A. Greco and E. Enrico, "Superconducting Josephson-based metamaterials for quantum-limited parametric amplification: a review" in Condensed Matter Physics, InTech Open, 2019.
4.
C. Guarcello et al., "Modeling of Josephson Traveling Wave Parametric Amplifiers", *IEEE Transactions on Applied Superconductivity*, vol. 33, no. 1, pp. 1-7, Jan. 2023.
5.
L. Fasolo et al., "Josephson Traveling Wave Parametric Amplifiers as non-classical light source for Microwave Quantum Illumination", *Measurement: Sensors*, vol. 18, pp. 100349, 2021.
6.
P. Livreri et al., "Microwave Quantum Radar using a Josephson Traveling Wave Parametric Amplifier", *2022 IEEE Radar Conference (RadarConf22)*, pp. 1-5, 2022.
7.
M. Esposito, A. Ranadive, L. Planat and N. Roch, "Perspective on traveling wave microwave parametric amplifiers", *Applied Physics Letters*, vol. 119, no. 12, pp. 09, 2021.
8.
A. Giachero et al., "Detector Array Readout with Traveling Wave Amplifiers", *Journal of Low Temperature Physics*, 2022.
9.
K. O'Brien, C. Macklin, I. Siddiqi and X. Zhang, "Resonant phase matching of Josephson junction traveling wave parametric amplifiers", *Phys. Rev. Lett.*, vol. 113, pp. 157001, Oct 2014.
10.

A. B. Zorin, "Josephson traveling-wave parametric amplifier with three-wave mixing", *Phys. Rev. Appl.*, vol. 6, pp. 034006, Sep 2016.
11.
L. Fasolo et al., "Bimodal approach for noise figures of merit evaluation in quantum-limited Josephson traveling wave parametric amplifiers", *IEEE Transactions on Applied Superconductivity*, vol. 32, no. 4, pp. 1-6, 2022.
12.
L. Ranzani, L. Spietz, Z. Popovic and J. Aumentado, "Two-port microwave calibration at millikelvin temperatures", *Review of Scientific Instruments*, vol. 84, no. 034704, 2013.
13.
A. Greco, L. Fasolo, A. Meda, L. Callegaro and E. Enrico, "A quantum model for rf-SQUIDs based metamaterials enabling 3WM and 4WM Travelling Wave Parametric Amplification", *Phys. Rev. B*, vol. 104, pp. 184517, 2021.